

Fourier Band-Power E/B-mode Estimators for Cosmic Shear

Matthew R. Becker^{1,2,*} and Eduardo Rozo^{2,3}

¹KIPAC, Physics Department, Stanford University, Stanford, CA 94305

²KIPAC, SLAC National Accelerator Laboratory, Menlo Park, CA 94025

³Department of Physics, University of Arizona, Tucson, AZ 85721

ABSTRACT

We introduce new Fourier band-power estimators for cosmic shear data analysis and E/B-mode separation. We consider both the case where one performs E/B-mode separation and the case where one does not. The resulting estimators have several nice properties which make them ideal for cosmic shear data analysis. First, they can be written as linear combinations of the binned cosmic shear correlation functions. Second, they account for the survey window function in real-space. Third, they are unbiased by shape noise since they do not use correlation function data at zero separation. Fourth, the band-power window functions in Fourier space are compact and largely non-oscillatory. Fifth, they can be used to construct band-power estimators with very efficient data compression properties. In particular, we find that all of the information on the parameters Ω_m , σ_8 and n_s in the shear correlation functions in the range of $\sim 10 - 400$ arcminutes for single tomographic bin can be compressed into only three band-power estimates. Finally, we can achieve these rates of data compression while excluding small-scale information where the modeling of the shear correlation functions and power spectra is very difficult. Given these desirable properties, these estimators will be very useful for cosmic shear data analysis.

Key words: gravitational lensing: weak; cosmology: theory; methods: data analysis

1 INTRODUCTION

Cosmic shear, or the weak gravitational lensing of background galaxies by large-scale structure, is one of the most promising cosmological probes because it can in principle provide direct constraints on the amplitude and shape of the projected matter power spectrum. Through measuring the growth of the matter power spectrum, cosmic shear will provide strong constraints on the nature of Dark Energy (e.g., Weinberg et al. 2013), interesting parameters like neutrino masses (e.g., Kitching et al. 2008) and new ideas like modifications to General Relativity (e.g., Beynon et al. 2010). Motivated by the intrinsic statistical power of cosmic shear measurements, a large number of surveys are either ongoing or have been planned in part to take cosmic shear measurements, including the DES¹, HSC², KIDS³, Pan-STARRS⁴, Euclid⁵, LSST⁶ and WFIRST⁷.

It is expected that these cosmic shear experiments will be diffi-

cult, being subject to many potential systematic effects in both the measurements and the modeling (see, e.g., Weinberg et al. 2013, for a review). Cosmic shear measurements are made by correlating the lensed shapes of galaxies with one another. As galaxies are approximately, but not exactly (see, e.g., Troxel & Ishak 2014, for a review), randomly oriented in the absence of lensing, we can attribute large-scale correlations among the galaxy shapes to gravitational lensing. However, we observe galaxies through the atmosphere and telescope which change their shapes through the point spread function (PSF). These instrumental effects can potentially be much bigger than the signals we are looking for and can mimic true cosmic shear signals. Thus they must be removed carefully.

Luckily, cosmic shear has several built-in null tests than can be used to search for and verify the absence of contamination in the signals. Checking for B-mode contamination in the cosmic shear signals is one of the most important of these null tests (Kaiser 1992). Weak gravitational lensing at the linear level only produces parity-free E-mode shear patterns. Small amounts of shear patterns with net handedness, known as B-mode patterns, can be produced by higher-order corrections, but their amplitude is generally much too small to be observed by current surveys (e.g., Krause & Hirata 2010). Thus we can use the absence or presence of B-mode patterns in the observed shear field to look for systematic errors. PSF patterns generally have similar levels of E- and B-modes unlike true cosmic shear signals. Note that ensuring the level of B-modes in a survey is consistent with zero is a necessary but not sufficient condition for the shear measurements to be error free. Other tests, such

* E-mail: beckermr@stanford.edu

¹ The Dark Energy Survey - <http://www.darkenergysurvey.org>

² Hyper Suprime-Cam - <http://www.naoj.org/Projects/HSC>

³ The Kilo Degree Survey - <http://kids.strw.leidenuniv.nl>

⁴ The Panoramic Survey Telescope & Rapid Response System - <http://pan-starrs.ifa.hawaii.edu>

⁵ <http://sci.esa.int/euclid>

⁶ Large Synoptic Survey Telescope - <http://www.lsst.org>

⁷ Wide-Field Infrared Survey Telescope - <http://wfirst.gsfc.nasa.gov>

as correlating the measured shears with the PSF itself, may provide a more powerful check on the level of systematic contamination (Heymans et al. 2012).

The importance of checking cosmic shear signals for B-mode contamination has motivated a large amount of work on devising statistical measures of the B-mode contamination (e.g., Schneider et al. 1998; Seljak 1998; Hu & White 2001; Schneider et al. 2002a; Schneider & Kilbinger 2007; Schneider et al. 2010; Hikage et al. 2011; Becker 2013). The main obstacle confronting every B-mode estimator is the mixing of E/B-modes in the estimator and the effect of ambiguous modes. This mixing happens on large-scales when one considers instead of an infinitely large survey, a survey of finite size. For a finite sized survey, modes with wavelengths of order the patch size can sometimes not be uniquely classified as either E- or B-modes (e.g., Bunn 2003). These ambiguous modes can contaminate the E- and B-mode estimators. If all of the power in the survey is sourced by E-modes, then the ambiguous modes are actually E-modes which then leads to mixing of E-modes into B-modes. Note also that masking, binning and pixelization can also produce E- to B-mode mixing (e.g., Smith 2006; Lin et al. 2012; Becker 2013).

In this work, we present extensions to the estimators derived in Becker (2013, B13 hereafter). The estimators presented in B13 use linear combinations of the binned real-space shear two-point correlation function measurements over a finite angular range excluding zero (see below) to produce statistics which optimally separate E- and B-modes. They additionally have the interesting property that given any linear combination of just the ξ_+ correlation function (see the definitions below), one can derive through a simple linear algebra the corresponding linear combination for ξ_- which maximizes the E- and B-mode separation. We will exploit this freedom to derive linear combinations of the binned real-space correlation function measurements which are local in Fourier space and optimally separate E- and B-modes. These Fourier space band-powers are competitive with more sophisticated pseudo- C_ℓ methods, producing as much or more separation between E- and B-modes (~ 4 orders of magnitude) while retaining the main advantage of shear correlation function measurements – accounting for the survey mask in real space.

Additionally, we derive below estimators which do not attempt to separate E- and B-modes, but instead assume all of the power is sourced by E-modes. They again use linear combinations of the binned shear correlation function data points to estimate a Fourier-space band-power. As the B-mode null test may not be the most powerful test of systematic contamination in cosmic shear measurements, we expect that these estimators will be useful for the analysis of cosmic shear data which has negligible systematic contamination.

We note that the band-powers presented in this work use apodized windows in Fourier space and explicitly account for the binning of the cosmic shear correlation functions, unlike those presented in Asgari & Schneider (2014). These features decrease the spillage and ringing of the band-powers and make the analysis exact in the sense that the estimators account for the full effects of the survey window function. Due to the fact that the band-power window functions in Fourier space can be computed exactly with the formalism presented in this work, they thus have no biases which impact a cosmological analysis. One simply uses the correct window functions to do the theoretical predictions and compute covariances.

Finally, we show that the estimators presented in this work can be used to construct band-powers with very efficient data compression properties, while remaining reasonably well-localized in both

real and Fourier space. We find that all of the information on the parameters Ω_m , σ_8 and n_s in the shear correlation functions from an angular range of $\sim 10 - 400$ arcminutes can be compressed into three band-powers. This conclusion is similar to those in Asgari & Schneider (2014). Performing cosmological parameter analysis in the data compressed space of band-powers can ease the requirements for generating large numbers of simulations for estimating covariances. While we have considered the data compression for only a single tomographic bin, further compression with our methods when doing full tomography should be possible as well.

This work is organized as follows. First we give an overview of the formalism of B13 and derive the new estimators in Section 2. Then we give two examples of the estimators and considerations for constructing them in Section 3. The data compression properties of the estimators are discussed in Section 3.3. Finally, we present discussion and conclusions in Section 4.

2 OPTIMAL ESTIMATORS FOR INPUT BAND WINDOWS

In this section, we use the methods of B13 to construct estimators for the lensing power spectra which are linear combinations of the shear two-point correlation functions. We consider two cases. First, we consider the case where no E/B-mode separation is performed. In this case, one is assuming explicitly that the weak lensing data is free of systematic errors (or at least systematic errors which would cause B-modes). Second, we consider the case where E/B-mode separation is performed, but one still wants an estimate of the power spectrum constructed from the two-point shear correlation functions. Note that estimators derived below are very similar to those presented in Schneider et al. (2002b) and the formalism below is very similar to that presented in Asgari & Schneider (2014). However, in this work we treat the binning of the cosmic shear correlation functions explicitly and further present apodized band-powers that exhibit less ringing than those presented in Asgari & Schneider (2014).

Before, considering the two cases outlined above, we review key parts of the formalism of B13. Suppose one constructs estimators X_\pm from the shear two-point functions as follows,

$$X_\pm = \frac{1}{2} \sum_i F_{+i} \hat{\xi}_{+i} \pm F_{-i} \hat{\xi}_{-,i}, \quad (1)$$

with

$$\hat{\xi}_{\pm i} = \int_{L_i}^{H_i} d\theta W_i(\theta) \xi_{\pm}(\theta). \quad (2)$$

Here the window functions, $W_i(\theta)$, are assumed to be normalized to unity over the angular range considered, $\theta \in [L_i, H_i]$. See B13 for a more extensive discussion of the window functions. For purely geometric effects, note that $W_i(\theta) = 2\theta/(H_i^2 - L_i^2)$. Finally, recall that the shear correlation functions can be written as (cf. Schneider & Kilbinger 2007)

$$\xi_+(\theta) = \int_0^\infty \frac{d\ell \ell}{2\pi} J_0(\ell\theta) [P_E(\ell) + P_B(\ell)] \quad (3)$$

$$\xi_-(\theta) = \int_0^\infty \frac{d\ell \ell}{2\pi} J_4(\ell\theta) [P_E(\ell) - P_B(\ell)] \quad (4)$$

where the $J_n(\ell\theta)$ are cylindrical Bessel functions. $P_E(\ell)$ and $P_B(\ell)$ are the E- and B-mode power spectra respectively.

Given the definitions above, we can write the expectation

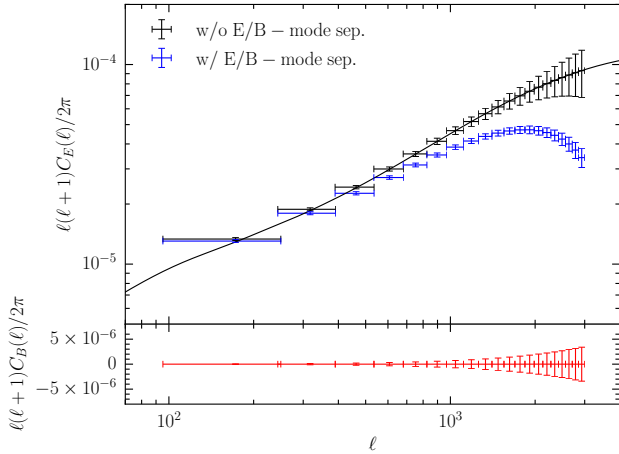


Figure 1. Band-power estimators which do not (black points) and do (blue and red points) separate E- and B-modes. Each estimator is shown with x-axis error bars giving the 1σ width of the log-Normal band window function and y-axis error bars giving the 1σ error on the band-power amplitude for a DES-like survey assuming all sources are at redshift one and using only Gaussian covariances for the cosmic shear correlation functions. The top panel shows the E-mode estimators and the bottom panel shows the B-mode estimators. The solid line is the underlying lensing power spectrum.

value of this estimator in terms of the E- and B-mode power spectra as

$$\langle X_{\pm} \rangle = \int_0^{\infty} d\ln \ell \left[\frac{\ell^2 P_E(\ell)}{2\pi} W_{\pm}(\ell) + \frac{\ell^2 P_B(\ell)}{2\pi} W_{\mp}(\ell) \right] \quad (5)$$

with

$$W_{\pm}(\ell) = \frac{1}{2} \sum_i \left(F_{+i} \int_{L_i}^{H_i} d\theta W_i(\theta) J_0(\ell\theta) \pm F_{-i} \int_{L_i}^{H_i} d\theta W_i(\theta) J_4(\ell\theta) \right).$$

B13 showed that the following steps lead to estimators which optimally separate E- and B-modes (where optimal here means that the estimators minimize E/B mixing in the root-mean-square sense for the window function $W_{\pm}(\ell)$; see B13).

- (i) Pick a fiducial F_{+} vector.
- (ii) Project out, as vectors, the quantities F_{+a} and F_{+b} from F_{+} . Note that these vectors correspond to ambiguous modes which cannot uniquely be classified as either E- or B-modes on a finite patch of sky. We denote the component of F_{+} orthogonal to the ambiguous modes as \tilde{F}_{+} .
- (iii) Compute F_{-} from \tilde{F}_{+} via a vector-matrix multiplication, $F_{-} = M_{+} \tilde{F}_{+}$.

B13 additionally demonstrated that this process can be repeated starting with F_{-} , with ambiguous modes F_{-a} and F_{-b} along with the matrix M_{-} .

For completeness, we reproduce the definitions of F_{+a} , F_{+b} , F_{-a} , F_{-b} , M_{+} and M_{-} below.

$$F_{+a} = \left(\int_{L_1}^{H_1} d\theta W_1(\theta), \int_{L_2}^{H_2} d\theta W_2(\theta), \dots, \int_{L_N}^{H_N} d\theta W_N(\theta) \right)_N \quad (6)$$

$$F_{+b} = \left(\int_{L_1}^{H_1} d\theta W_1(\theta) \theta^2, \int_{L_2}^{H_2} d\theta W_2(\theta) \theta^2, \dots, \int_{L_N}^{H_N} d\theta W_N(\theta) \theta^2 \right)_N \quad (7)$$

$$F_{-a} = \left(\int_{L_1}^{H_1} d\theta \frac{W_1(\theta)}{\theta^2}, \int_{L_2}^{H_2} d\theta \frac{W_2(\theta)}{\theta^2}, \dots, \int_{L_N}^{H_N} d\theta \frac{W_N(\theta)}{\theta^2} \right)_N \quad (8)$$

$$F_{-b} = \left(\int_{L_1}^{H_1} d\theta \frac{W_1(\theta)}{\theta^4}, \int_{L_2}^{H_2} d\theta \frac{W_2(\theta)}{\theta^4}, \dots, \int_{L_N}^{H_N} d\theta \frac{W_N(\theta)}{\theta^4} \right)_N \quad (9)$$

$$(M_{+})_{ki} = \delta_{ki} + \left(\int_{L_k}^{H_k} d\theta \frac{W_k^2(\theta)}{\theta} \right)^{-1} \times \int_{L_i}^{H_i} \int_{L_k}^{H_k} d\theta d\phi W_i(\theta) W_k(\phi) \times \left(\frac{4}{\phi^2} - \frac{12\theta^2}{\phi^4} \right) H(\phi - \theta) \quad (10)$$

$$(M_{-})_{ki} = \delta_{ki} + \left(\int_{L_k}^{H_k} d\theta \frac{W_k^2(\theta)}{\theta} \right)^{-1} \times \int_{L_i}^{H_i} \int_{L_k}^{H_k} d\theta d\phi W_i(\theta) W_k(\phi) \times \left(\frac{4}{\theta^2} - \frac{12\phi^2}{\theta^4} \right) H(\theta - \phi) \quad (11)$$

In these expressions $H(\theta)$ is the Heaviside step function and δ_{ki} is the Kronecker delta function. See B13 for a detailed explanation of how these quantities are defined and derived.

2.1 Estimators without E/B-mode Separation

Imagine the case where one has a target band-power window, $W_T(\ell)$, which is used to produce a band-power estimate of the shear power spectrum,

$$D_T = \int_0^{\infty} \frac{d\ell}{2\pi} W_T(\ell) P_E(\ell). \quad (12)$$

Note that for piecewise-constant power spectra, P_{α} , over some range in $\ell \in [L_{\alpha}, H_{\alpha}]$, this band-power is

$$D_{\alpha} = P_{\alpha} \int_{L_{\alpha}}^{H_{\alpha}} \frac{d\ln \ell}{2\pi} \ell^2 W_{\alpha}(\ell). \quad (13)$$

We define estimators which optimally match the target window function $W_T(\ell)$ by minimizing the squared difference between the output window function and the test window function,

$$\int_0^{\infty} d\ell \ell [W_T(\ell) - W_{+}(\ell)]^2. \quad (14)$$

See Asgari & Schneider (2014) for the unbinned version of the derivation below. Minimizing the expression above with respect to

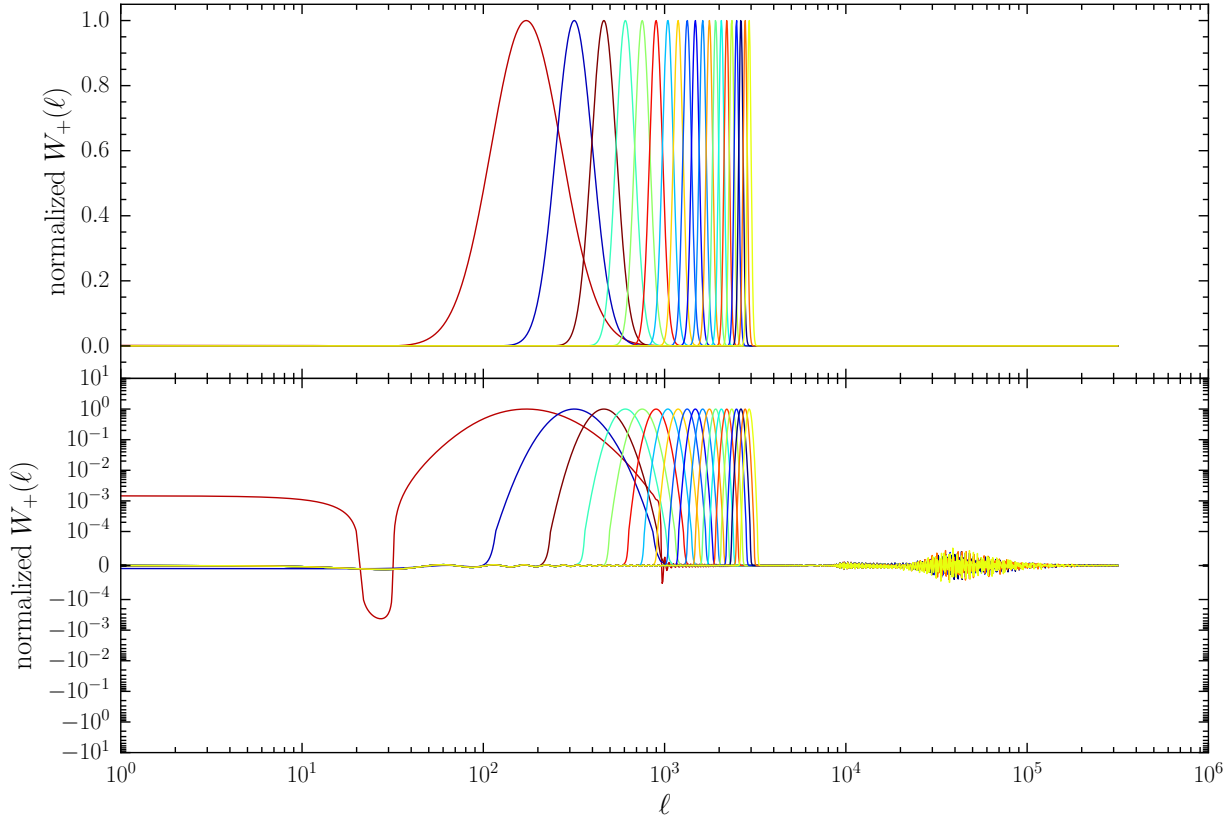


Figure 2. Band-power estimator kernels $W_+(\ell)$ with no E/B-mode separation. Each color shows a different band-power estimators with a linear scale (top) and symmetric log-scale (bottom). The scaling in the bottom panel is logarithmic above/below $\pm 10^{-4}$, but linear between. Each kernel has been normalized to unity at its peak. Note that the wings of the band-powers are both positive and negative so that under integration they largely cancel out.

F_+ and F_- simultaneously (see B13 for similar algebraic manipulations), we get the following linear equations

$$F_+ = A^0 - M_- F_- \quad (15)$$

$$F_- = A^4 - M_+ F_+ . \quad (16)$$

We can solve these equations for F_+ , getting

$$(I - M_- M_+) F_+ = A^0 - M_- A^4 . \quad (17)$$

Here the $A^{0,4}$ vectors are

$$A_k^0 = 2 \left[\int_{L_k}^{H_k} d\theta W_k^2(\theta)/\theta \right]^{-1} \times \int_{L_k}^{H_k} d\theta \int_0^\infty d\ell \ell W_k(\theta) W_T(\ell) J_0(\ell\theta) \quad (18)$$

$$A_k^4 = 2 \left[\int_{L_k}^{H_k} d\theta W_k^2(\theta)/\theta \right]^{-1} \times \int_{L_k}^{H_k} d\theta \int_0^\infty d\ell \ell W_k(\theta) W_T(\ell) J_4(\ell\theta) \quad (19)$$

Once F_+ is known, we can solve for F_- trivially using Equation (16) above. Note that the existence of this estimator requires that the matrix $I - M_- M_+$ be invertible or equivalently have an

empty kernel or null space. As demonstrated in B13, for the geometric window functions defined above and logarithmic shear correlation function binning, this matrix is typically invertible (B13 tested only specific cases and did not provide a general proof). Thus we expect these estimators to exist for most surveys, but note that their detailed properties depend on the survey window functions, specific binning, etc.

2.2 Estimators which Separate E- and B-modes

We define a heuristic method to construct estimators which simultaneously match the test window function $W_T(\ell)$ and separate E- and B-modes. To do this, we just optimize the metric above for F_+ and set F_- by minimizing the E/B-mixing, using the steps listed above. Then we get

$$[I + M_- M_+ (I - \tilde{F}_{+a} \tilde{F}_{+a}^T - \tilde{F}_{+b} \tilde{F}_{+b}^T)] F_+ = A^0 \quad (20)$$

and $F_- = M_+ \tilde{F}_+ = M_+ (I - \tilde{F}_{+a} \tilde{F}_{+a}^T - \tilde{F}_{+b} \tilde{F}_{+b}^T) F_+$. Here we have defined projection operators for the ambiguous modes as $F_{+a} F_{+a}^T$ and $F_{+b} F_{+b}^T$. The vectors \tilde{F}_{+a} and \tilde{F}_{+b} are just the ambiguous modes, but rewritten so that they are mutually orthogonal and normalized to unity.

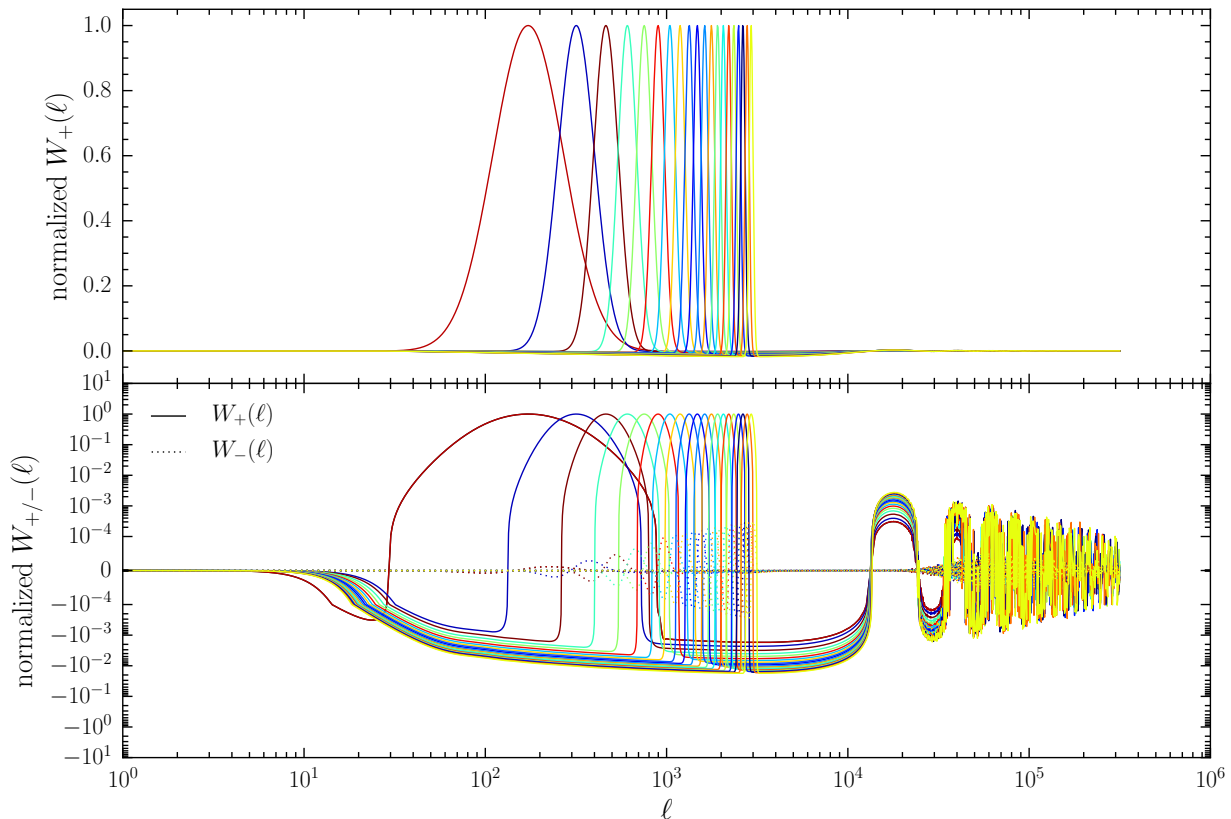


Figure 3. Band-power estimator kernels $W_{+/-}(\ell)$ with E/B-mode separation. Each color shows a different band-power estimators with a linear scale (top) and symmetric log-scale (bottom). The scaling in the bottom panel is logarithmic above/below $\pm 10^{-4}$, but linear between. Each kernel has been normalized to unity at its peak, with the $W_{-}(\ell)$ kernels normalized by the peak of the corresponding $W_{+}(\ell)$ kernels, so that the relative amplitudes are correct. In the bottom panel, the dotted lines show the $W_{-}(\ell)$ filters. Mixing between E- and B-modes is controlled by the amplitude of the $W_{-}(\ell)$ kernel, which is suppressed by $\sim 3 - 4$ orders of magnitude.

3 EXAMPLE SETS OF ESTIMATORS

We now give two example sets of estimators in order to illustrate their performance and to further discuss design considerations. Specifically, we construct estimators of both types discussed above. For concreteness, we consider a survey which has measured shear correlation function data in 10^3 angular bins between 1 and 400 arcminutes. We also use the geometric bin window functions given above.

3.1 Considerations for Choosing $W_T(\ell)$

In this work, we use a log-normal target window in Fourier space

$$W_T(\ell) = \frac{1}{\sigma\sqrt{2\pi}} \exp \left[-\frac{1}{2} \left(\frac{\log \ell - \log \ell_m}{\sigma} \right)^2 \right]. \quad (21)$$

We set ℓ_m to be spaced linearly,

$$\ell_{m,i+1/2} = \Delta\ell(i + 1/2) + \ell_{min}$$

where $\Delta\ell = (\ell_{max} - \ell_{min})/N$, with $\sigma = \log(\ell_{m,i+1}/\ell_{m,i})/2$. We have found empirically that these choices for the target band windows produce locally compact estimators which minimize ring-

ing in Fourier space. We use $\{\ell_{min}, \ell_{max}, N\} = \{100, 3000, 20\}$ in this work. Other target window functions, like apodized top-hat band windows also work well, but we do not consider those choices in this work.

3.2 The Estimators

The band-power estimators with their expected errors, assuming Gaussian covariances for a DES-like survey (see Section 3.3) are shown in Figure 1. We have assumed all sources are at redshift one for this computation. We show for each band-power the 1σ width of the window function and the 1σ error bar assuming the DES-like survey. The band-powers which do not separate E- and B-modes (black points) track the underlying power spectrum (solid line) closely. For estimators which separate E- and B-modes (blue points), there is a feature due to the estimator window functions at high- ℓ . The window functions for estimators which separate E- and B-modes exhibit some degree of compensation (due to the removal of the ambiguous modes) and thus at high- ℓ deviate in the mean from the underlying power spectrum. Note however that this deviation can be predicted exactly so that parameter estimator done with these estimators will still result in unbiased parameters (as-

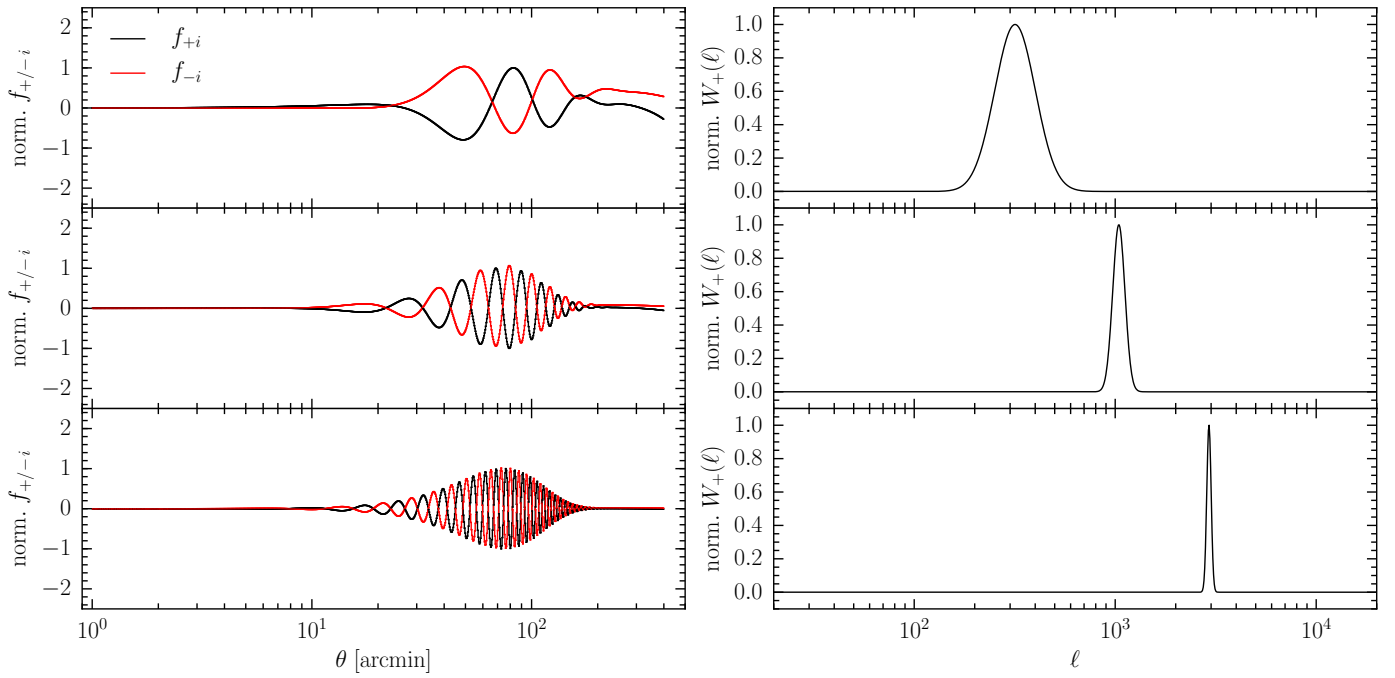


Figure 4. The real-space weights $f_{+/-i}$ (left) and corresponding Fourier space window functions (right) for three selected band-power estimators which do not separate E- and B-modes. As expected, as the Fourier space window targets higher ℓ modes, more oscillations appear in real space. Once the real-space oscillations exceed the local Nyquist frequency of the real-space correlation function binning, the estimators begin to show significant ringing in Fourier space.

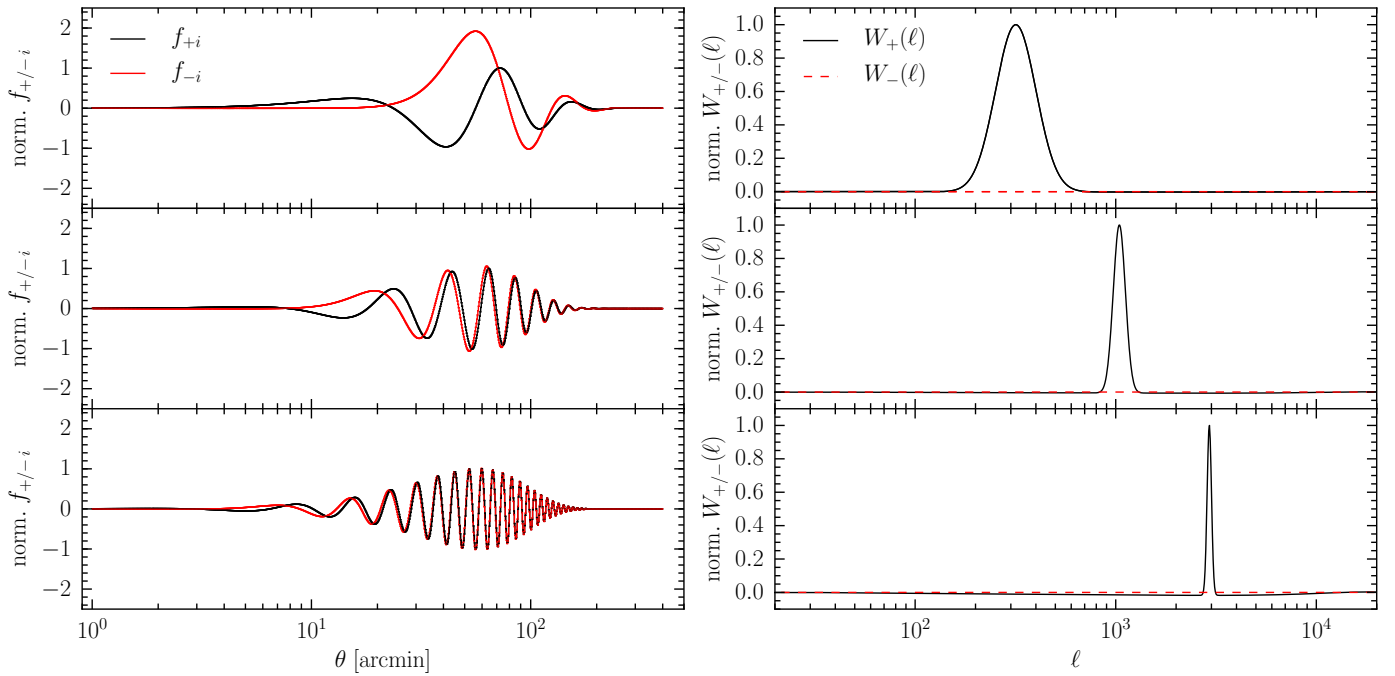


Figure 5. The real-space weights $f_{+/-i}$ (left) and corresponding Fourier space window functions (right) for three selected band-power estimators which separate E- and B-modes. As expected, as the Fourier space window targets higher ℓ modes, more oscillations appear in real space. Once the real-space oscillations exceed the local Nyquist frequency of the real-space correlation function binning, the estimators begin to show significant ringing in Fourier space.

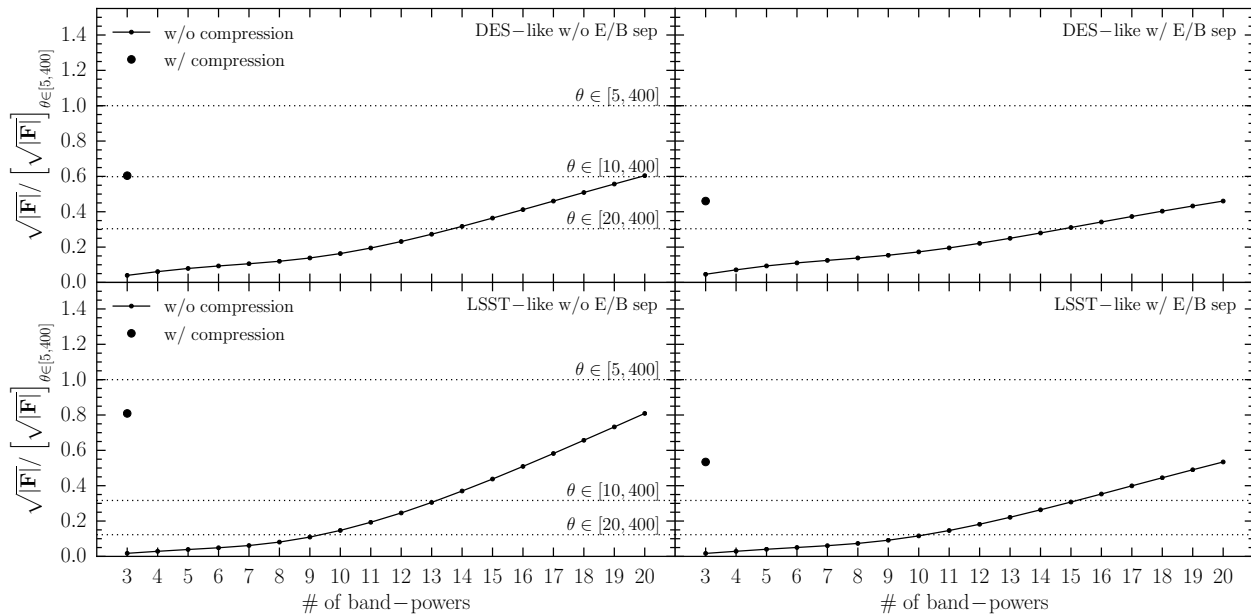


Figure 6. The Fisher information content of band-power estimators for DES- (top) and LSST-like (bottom) surveys. Estimators without E/B-mode separation are on the left and estimators with E/B-mode separation are on the right. The solid line shows the information content in the case of no data compression. The information content of the compressed statistics is shown by the large solid point. The dotted lines from bottom top show the amount of information contained in a shear correlation function only analysis as a function of the smallest scale considered from 20 to 5 arcminutes. Note that the band-power estimators generally assign very little weight to shear correlation function data below 10 arcminutes, but that the conversion between Fourier mode and angular scale is not exact.

suming no other biases of course). The bottom panel of this figure shows the B-mode band-powers (red points) which are suppressed by ~ 4 orders of magnitude relative to the E-mode estimators. This level of separation between the band-powers is competitive with standard pseudo- $C(\ell)$ methods (e.g., Hikage et al. 2011).

Figures 2 and 3 show the window functions $W_{+/-}(\ell)$ for estimators which don't or do separate E- and B-modes respectively. In general, the window functions are quite compact in Fourier space, but they do however exhibit oscillations for large ℓ . Fortunately, the regions which exhibit these oscillations are suppressed by factor of 10^2 to 10^3 relative to the peak and under integration these oscillations will largely cancel. Additionally, for estimators which separate E- and B-modes, the $W_{-}(\ell)$ kernels are suppressed by $\sim 3 - 4$ orders of magnitude, indicating that these estimators have a very small amount of E/B mixing.

We show the real-space filters for these estimators in Figures 4 and 5 for estimators which don't or do separate E- and B-modes respectively. We find unsurprisingly that as the target band window function moves higher in ℓ , there are more oscillations in the real-space weights $f_{+/-i}$. Additionally, we find that if the oscillations in the real-space weights exceed the local Nyquist frequency of the real-space correlation function binning, the estimators being to show significant non-locality in Fourier space. This consideration motivates the choice of the number of real-space bins to use to construct the estimators. We have chosen 10^3 for this example, but note that for estimators up to $\ell \sim 1000$, 500 bins in real-space works reasonably well too. Finally, note that one must have a sufficient number density of sources in order to use a large number of radial bins. Assuming one needs at minimum 10^3 source pairs in a radial bin, then for a radial bin at 1 arcminutes with a $\sim 0.6\%$ width (the width used in this work for 10^3 bins in the range 1 to 400 ar-

cminutes) for a DES-like survey, one requires a source density of at least ~ 0.01 galaxies per square arcminute. All future lensing surveys clearly meet this requirement.

Notice that in real-space, these estimators are very efficient at excluding small-scale modes in the shear correlation functions. Thus these estimators can be used to help render cosmic shear measurements insensitive to potential systematic effects on small scales, like baryonic effects in the matter power spectrum (e.g., Zhan & Knox 2004; White 2004; Rudd et al. 2008; van Daalen et al. 2011; Casarini et al. 2012) or the small-scale selection effects in shear measurements (e.g., Hartlap et al. 2011). Similarly, these estimators do not use the shear correlation functions at zero separation, rendering them unbiased by shape noise.

3.3 Fisher Information Content and Data Compression

In this section we compute the Fisher information content in the band-power estimators and explore how efficiently these estimators can compress the shear correlation function data. We use a Λ CDM cosmological model with $\Omega_m = 0.25$, $H_0 = h^{-1}100 \text{ km s}^{-1} \text{ Mpc}^{-1}$, $h = 0.7$, $\sigma_8 = 0.8$, $n_s = 1.0$ and $\Omega_b = 0.044$. We consider only the Gaussian and shape noise contributions to the covariance matrix of the shear correlation functions, use the Smith et al. (2003) fitting function for the non-linear power spectrum, and the Eisenstein & Hu (1998) fitting formula for the transfer function. We additionally consider both DES- and LSST-like surveys with source densities \bar{n} and areas Ω_s of $(\bar{n}, \Omega_s) = (10 \text{ galaxies/arcmin}^2, 5,000 \text{ deg}^2)$ and $(\bar{n}, \Omega_s) = (40 \text{ galaxies/arcmin}^2, 20,000 \text{ deg}^2)$ respectively. Finally, we fix all lensing sources to redshift 1.

We use as a metric for the information content of the survey, $f = \sqrt{|\mathbf{F}|}$, the square root of the determinant of the Fisher infor-

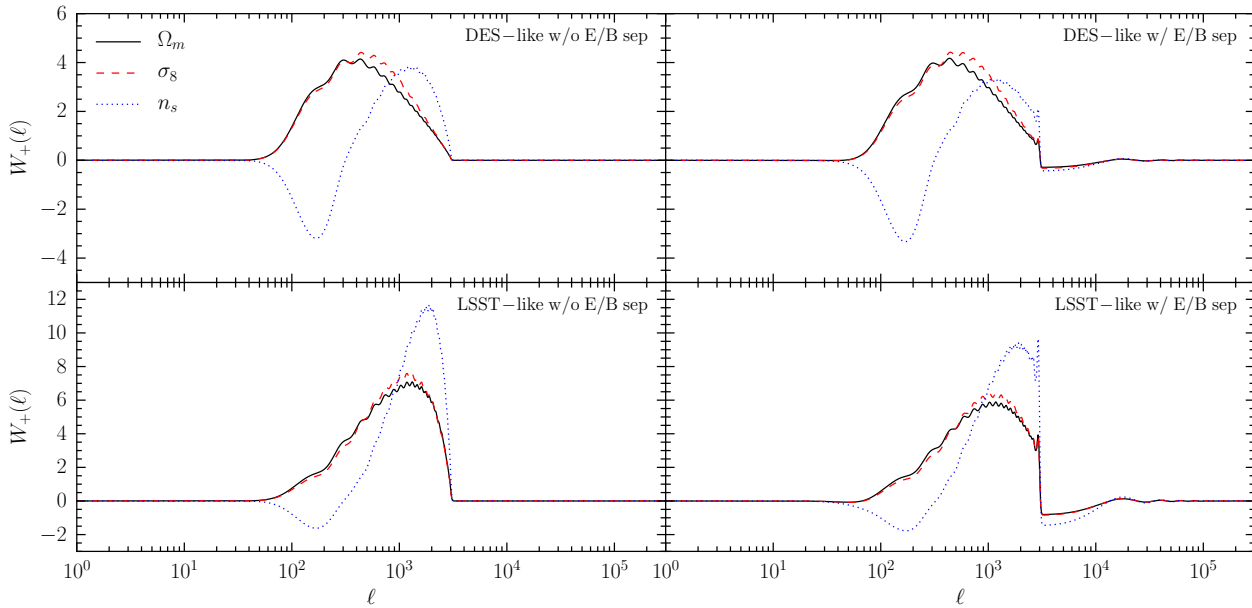


Figure 7. Band-power window functions $W_+(\ell)$ for the optimally compressed statistics for Ω_m (black solid), σ_8 (red dashed) and n_s (blue dotted). We show results for a DES-like survey in the top panels and an LSST-like survey in the bottom panels. The case of no E/B-mode separation is shown in the left column and the case with E/B-mode separation is shown in the right column.

mation matrix. As we are using a single source plane, we consider the information content only in Ω_m , σ_8 and the spectral index n_s . See B13 for the details of the Fisher matrix computation. We leave the exploration of data compression methods for tomographic lensing analyses for future work. However, note that to the extent that the majority of the extra information in a tomographic as compared to a non-tomographic analysis comes from the relative amplitudes of the shear correlation functions or power spectra as a function of redshift, we expect results for a single source plane to still be useful since they represent the amount of data compression possible in any given tomographic bin. The data compression possible for the entire tomographic analysis can then be estimated by straight forward combinatorics, though this estimate should be too pessimistic. These issues have been explored in Asgari & Schneider (2014) where further data compression in the case of tomography was possible.

We show the results of our Fisher matrix analysis in Figure 6. Here we show the amount of Fisher information, characterized by f , as a function of the number of band-powers used (where the band-powers are ordered by lowest Fourier mode to highest) for both a DES-like and LSST-like survey. For comparison, we show the amount of information directly in the shear correlation functions as a function of the smallest angular scale considered, from 20 to 5 arcminutes, with the dotted lines. In general, the amount of information increases greatly as smaller scales are considered, as is well known in weak lensing (e.g., Takada & Jain 2009). The band-power estimators generally have very little weight below ≈ 5 –10 arcminutes. We find that with as few as ~ 10 –20 band-powers, we can recover the majority of the information in the shear correlation functions above 10 arcminutes. Note that the estimators with E/B-mode separation are less well localized in Fourier space. Their high- ℓ tails, even though they exhibit oscillations, contribute to the total Fisher information content so that they can give a more effi-

cient data compression at the cost of having less control of which scales are used.

Finally, we consider a nearly optimal data compression scheme, following Tegmark et al. (1997). First, note that the Fisher information matrix can be written as (e.g., Tegmark et al. 1997)

$$F_{ij} = \frac{1}{2} \text{Tr} [C^{-1} (\bar{\mu}_{,i} \bar{\mu}_{,j}^T + \bar{\mu}_{,j} \bar{\mu}_{,i}^T)] . \quad (22)$$

where C is the covariance matrix and $\bar{\mu}_{,i}$ is the derivative of the mean data values with respect to parameter i . For a single parameter, it is clear that the linear combination of data points which contributes most to the trace of the quantity in brackets will contain the most information about the parameter under consideration. Thus if we decompose the matrix in the brackets into its eigenvalues and eigenvectors, we can perform nearly optimal data compression by retaining only the linear combination of data points given by the eigenvalue and eigenvector pair with the largest eigenvalue. For multiple parameters, we choose to simply retain the most efficient linear combination for each parameter considered separately. Note that the exact set of optimal linear combinations depends both on the analysis under consideration and the properties of the survey, which are all encoded in the data vectors and their covariance matrix. Also, one should be able to compute the optimal set of statistics from approximate covariance matrices, like those from the halo model applied to cosmic shear (e.g., Takada & Jain 2009), as opposed to covariance matrices computed directly from simulations (see also Asgari & Schneider 2014). We leave the exploration of these specific issues to future work and instead give below an example of potential amount of data compression possible.

We use the process outlined previously to find the three linear combinations of the band-power estimators which retain the most information on Ω_m , σ_8 and n_s . The solid point line in Figure 6 shows the amount of information in just these three linear combinations. We find that with just these linear combinations of the band-powers, we can retain essentially all of the information in all

twenty of the band-powers used in this work. In Figure 7, we show the effective band-power Fourier space windows for the three compressed statistics. These are quite similar to those found by Asgari & Schneider (2014). Note that the window function for n_s is both positive and negative as expected. We have repeated this analysis with just σ_8 and Ω_m and find that all of the information in the band-powers on these parameters can be compressed into just two statistics. Finally, in agreement with Asgari & Schneider (2014), we find that the amount of data compression is only changed by at most a few percent in f when using a different cosmology ($\Omega_m = 0.28$, $\sigma_8 = 0.84$ and $n_s = 0.96$, all other parameters are the same) to compute the compressed basis linear combinations.

4 CONCLUSIONS

In this work, we have derived two new sets of band-power estimators for cosmic shear power spectra. There are several key features of these estimators which we expect will make them quite useful for cosmic shear data analysis.

- (i) The band-powers can be written and computed as linear combinations of the *binned* real-space shear correlation functions and thus take the binning of the correlation functions into account explicitly.
- (ii) The covariance matrix of the band-powers can be derived directly from a linear transformation of the shear correlation function covariance matrix.
- (iii) The estimators account for the survey window function directly in real-space.
- (iv) The estimators do not use shear correlation function data at zero separation and are thus have no biases due to shape noise.
- (v) The window functions of the band-powers in ℓ -space are compact and largely non-oscillatory, making them easy to interpret. This feature also allows one to exclude regions of ℓ -space where models for the lensing power spectra may have significant uncertainties, due say to galaxy formation (see references above).
- (vi) These estimators can be used to construct very efficient data compression schemes with only three band-powers required to capture all of the information on the parameters Ω_m , σ_8 and n_s in the shear correlation functions in the range of $\sim 10 - 400$ arcminutes for single tomographic bin.

Importantly, the bin window functions $W_i(\theta)$ can be measured from the cosmic shear source galaxy positions themselves.⁸ This measurement is possible because the typical signal-to-noise of cosmic shear for a single galaxy pair is $\approx 0.01/(0.3\sqrt{2}) \approx 1/40$ whereas the signal-to-noise of the number of cosmic shear pairs as a function of angle (i.e., the unnormalized bin window function) is $1/\sqrt{1} = 1$. Thus the signal-to-noise of the bin window function measurement for any angular bin will always be $\approx 40\times$ higher than that of the cosmic shear correlation functions. Therefore incredibly low-noise measurements of the bin window functions can be made from the cosmic shear catalogs themselves. Given these practical considerations of their implementation and the features

listed above, we expect the estimators derived in this work to be quite useful for cosmic shear data analysis.

ACKNOWLEDGMENTS

MRB thanks Bhuvnesh Jain, Tim Eifler, Elisabeth Krause and Sarah Bridle for enlightening discussions of cosmic shear window functions. MRB and ER thank Scott Dodelson for helping to inspire this work. This work made extensive use of the NASA Astrophysics Data System and arXiv.org preprint server.

REFERENCES

- Asgari M., Schneider P., 2014, [arXiv:astro-ph/1409.0863](http://arXiv.org/astro-ph/1409.0863)
- Becker M. R., 2013, *MNRAS*, 435, 1547
- Beynon E., Bacon D. J., Koyama K., 2010, *MNRAS*, 403, 353
- Bunn E. F., 2003, *New A Rev.*, 47, 987
- Casarini L., Bonometto S. A., Borgani S., Dolag K., Murante G., Mezzetti M., Tornatore L., La Vacca G., 2012, *A&A*, 542, A126
- Eisenstein D. J., Hu W., 1998, *ApJ*, 496, 605
- Hartlap J., Hilbert S., Schneider P., Hildebrandt H., 2011, *A&A*, 528, A51
- Heymans C. et al., 2012, *MNRAS*, 427, 146
- Hikage C., Takada M., Hamana T., Spergel D., 2011, *MNRAS*, 412, 65
- Hu W., White M., 2001, *ApJ*, 554, 67
- Kaiser N., 1992, *ApJ*, 388, 272
- Kitching T. D., Heavens A. F., Verde L., Serra P., Melchiorri A., 2008, *Phys. Rev. D*, 77, 103008
- Krause E., Hirata C. M., 2010, *A&A*, 523, A28
- Lin H. et al., 2012, *ApJ*, 761, 15
- Rudd D. H., Zentner A. R., Kravtsov A. V., 2008, *ApJ*, 672, 19
- Schneider P., Eifler T., Krause E., 2010, *A&A*, 520, A116
- Schneider P., Kilbinger M., 2007, *A&A*, 462, 841
- Schneider P., van Waerbeke L., Jain B., Kruse G., 1998, *MNRAS*, 296, 873
- Schneider P., van Waerbeke L., Kilbinger M., Mellier Y., 2002a, *A&A*, 396, 1
- Schneider P., van Waerbeke L., Kilbinger M., Mellier Y., 2002b, *A&A*, 396, 1
- Seljak U., 1998, *ApJ*, 506, 64
- Smith K. M., 2006, *Phys. Rev. D*, 74, 083002
- Smith R. E. et al., 2003, *MNRAS*, 341, 1311
- Takada M., Jain B., 2009, *MNRAS*, 395, 2065
- Tegmark M., Taylor A. N., Heavens A. F., 1997, *ApJ*, 480, 22
- Troxel M. A., Ishak M., 2014, [arXiv:astro-ph/1407.6990](http://arXiv.org/astro-ph/1407.6990)
- van Daalen M. P., Schaye J., Booth C. M., Dalla Vecchia C., 2011, *MNRAS*, 415, 3649
- Weinberg D. H., Mortonson M. J., Eisenstein D. J., Hirata C., Riess A. G., Rozo E., 2013, *Phys. Rep.*, 530, 87
- White M., 2004, *Astroparticle Physics*, 22, 211
- Zhan H., Knox L., 2004, *ApJ*, 616, L75

This paper has been typeset from a \LaTeX file prepared by the author.

⁸ Note that it is the positions of these galaxies that define the cosmic shear window function. In other words, the cosmic shear window function answers the question where did we measure the shear field, not where we could have measured the shear field (which is the information carried in the tradition survey mask, but modified for the selection of cosmic shear sources).